Using Acoustic Emission Signal Categorization for Reconstruction of Wear Development Timeline in Tribosystems: Case Studies and Application Examples

Abstract

The purpose of this work is to demonstrate how a new acoustic emission (AE) technique can be used to monitor friction surface degradation in a four-ball tribosystem under different types of lubrication. The AE method is based on a novel signal spectral categorization technique, and it was used to identify concurrent degradation processes in bearing steel. The correlation of AE features with the development of specific microstructural features on the contact surfaces has been used to identify the AE "signature" of specific damage mechanisms, and thus to monitor the progression of wear. The proposed approach enables the construction of a chronology of lubricant and/or contacting material degradation during tribological testing with a high degree of confidence. Furthermore, it provides an efficient means for automated wear monitoring and for real-time, non-supervised interpretation of the state of wear in a given tribosystem.

1. Introduction

Tribological testing is routinely used to evaluate the performance of lubricants and properties of contacting materials. The behavior of lubricants is influenced, among other things, by various external factors such as load, temperature, and environment [1]. One of the primary objectives of tribology is optimization of friction processes leading to a reduction in material and energy losses and to the extension of the failure-free operation of machines and devices. To accomplish this goal, the details of non-damaging and damaging modes of operation of tribological contacts should be understood. More specifically, laboratory testing is often aimed at:

1) establishing the conditions under which the lubricant loses its protective properties; comparing and selecting lubricants

2) describing the stages of friction damage initiation and accumulation;

3) identifying the predominant wear mechanisms and the timing of their occurrence;

4) comparing the degradation behaviors of different contact pairs.

To address these objectives and to assess the behavior of a tribosystem, it is essential to know the time history of damage evolution since its inception to failure. Obtaining this information is challenging due to the inaccessibility of the friction contact area for direct observations during testing. The post-mortem investigation of the worn area yields only limited information, because of the compound effect of multiple damaging processes on the worn surface appearance. Therefore, the roles of individual mechanisms cannot be assessed separately at the end of the test. Alternative conventional indirect methods, such as the measurement of the friction force and temperature as well as interrupted testing for the mid-term visual observation and/or the measurement of the wear scar size are either not applicable, costly, or can adversely affect the results in many, if not most, practical cases. Therefore, novel approaches are required to get a better insight into temporal details of damage evolution *in-situ* without altering testing conditions or practically adopted standard test schedules.

The acoustic emission method (AE) has long been proven effective in gaining a deeper understanding of friction and wear processes in sliding and rolling contacts [2-7]. AE has often been reported to be more sensitive to damage process and operating conditions than the friction force [8] or vibration measurements [9]. Different ways of AE characterization have been explored, with different levels of success. The count rate, root mean square (*rms*) voltage or envelope were the AE features most frequently used in tribology [8, 10-18]. Despite the simplicity of these parameters, the empirical relationships have been found between them and the wear scar volume or the wear rate. However, a robust distinction between different damage mechanisms is hardly possible by means of these integral AE parameters. The recent rapid advent of information technologies and the increasing power of computing have opened new prospects for advanced data mining and machine learning techniques which take a prominent position in modern tribology studies, see, e.g. [3, 16, 19-21]. The use of spectral (Fourier [22, 23] or wavelet [24-27]) transform has shown that the frequency or time-frequency distribution of the AE power (energy) varies depending on friction conditions and this can be used for prediction of scuffing [28]. To increase further the efficiency of the AE spectral analysis, an original AE signal clustering algorithm based on a statistical comparison of AE spectral density functions is employed in the present work.

It has been well-understood that several mechanisms can be involved in a wear process concurrently [29]. Different individual mechanisms can interact in a sequential manner (or in parallel) to form a complex wear progression. The relative importance of individual wear mechanisms can change with the changes in influential parameters including metallurgy factors, testing conditions, and chemical factors. To gain a better understanding and to characterize the wear process in more details it is, therefore, important to distinguish between different modes of damage and to reconstruct the chronology of their occurrence. Thus, the AE method seems to be indispensable for addressing this challenge. In what follows a novel AE-based approach integrating continuous data acquisition, spectral analysis and statistical categorization of AE waveforms is described in the application to friction and wear condition monitoring. The proposed methodology allows to:

- reproduce the chronology of degradation of lubricants and contacting surfaces in tribological tests;
- automate the AE data recording and processing for routine practical testing;
- simplify the presentation of AE results for quick interpretation.

Four main wear situations between the contacting surfaces, which are commonly recognized in the literature, include adhesive wear, abrasion wear, fatigue wear, and tribochemical (corrosive) wear [30]. The present work deals primarily with adhesive wear although the proposed methodology can be adapted easily to other situations.

2. Method Implementation

The proposed workflow is shown in Fig. 2. The approach involves a Fourier spectral decomposition followed by statistical categorization (clustering) of individual spectra corresponding to AE sources of different origin. The signal categorization is applied in parallel with the traditional analysis of integral AE features discussed above. The active wear mechanism is associated with one of the pseudo-AE sources prevailing over the others in the sliding contact zone at a given time. In the present work, these sources are confined to the elastic and plastic interaction between asperities, micro-cutting, and scratching, adhesion and scuffing. Several typical examples illustrating the proposed methodology are given below.

3. Experimental Details

The proposed approach was validated during the investigation of the degradation of several contact materials under controlled lubrication conditions in the standard tribosystems: (1) four-ball [31, 32], (2) pin-on-disk [33] and (3) cylinder-on-ring [34] as shown schematically in Fig. 1. For the sake of brevity, the results of the four-ball testing of 100Cr6 steel balls will be mainly discussed in what follows. However, very similar results were obtained for other methods and materials as well.

Contacting materials included 12.7 mm diameter 100Cr6 steel balls (four-ball method); 6.0 mm diameter 100Cr6 steel balls, and 30×40×5 mm St35 and C45 steel plates (pin-on-disk method), 8 mm diameter 40CrNiMo22 steel, and AlMg3 type aluminum alloy cylinders, 50 mm diameter, 5 mm wide roller made of abrasion resistant Gh190 cast iron (cylinder-on-ring method).

Several lubrication conditions were simulated with different lubricants, such as motor oil and various commercial greases. Their codified designations and properties are summarized in Table 1.

AE recording was performed by using a home-built AE system, operating in the frequency range of 50 to 1000 kHz. A broadband AE-900S-WB transducer AE was mounted in the closest possible proximity to the sliding contact as shown schematically in Fig. 1. A total gain was set at 40 dB. Machine oil was used as a coupling medium to ensure efficient transfer of elastic waves from the surface to the transducer.

For integral AE characterization, a *waveform envelope* Y was measured by an analog integrator circuit built-in in the pre-amplifier as

$$Y = \frac{1}{T}\int_0^T \left|U(t)\right| dt, \tag{2}$$

where $U(t)$ is the voltage at the output of the preamplifier, and T is the integration time constant. The Y value was then recorded by the AE system in parallel with the waveform. The envelope integration time constant was set at 100 ms to eliminate spike-like noise. For the AE signal classification, the continuously recorded AE signal was sectioned into consecutive individual realizations (“frames”). Each frame contained n=8192 readings sampled at 6.25 MHz. The following parameters were computed for each frame: amplitude, energy and median frequency of the power spectral density (PSD). The *energy* (per frame) W is defined as the area below the AE PSD $G(f)$ curve given as a function of frequency f as:

$$W = \int_{f_{\min}}^{f_{\max}} G(f)\,df \,, \tag{3}$$

where $f_{\min}$ and $f_{\max}$ denote the minimum and maximum frequency in the frequency band of the acquisition system. The *median frequency* f_{m} of the PSD function is computed by definition as:

$$\int_{f_{\min}}^{f_{\mathrm{m}}} G(f)\,df = \int_{f_{\mathrm{m}}}^{f_{\max}} G(f)\,df \,. \tag{4}$$

The AE Fourier PSD was computed for each frame by using a periodogram method with the Hanning smoothing window of 50 kHz width [35]. Other popular methods for calculation of PSD, such as the Welch [36] technique, for example, can also be used without limitations.

A generally reasonable assumption, based on the fundamental theoretical considerations, is that different sources produce AE signals with different waveforms and corresponding PSDs. In application to tribology, this has been corroborated by the results by Hase et al. [23] who demonstrated that, in principle, the mechanisms of wear can be recognized from the features of AE frequency spectra. Since AE is a random process, some regular scatter is inevitable in the estimates of waveforms or in their spectra. This makes it difficult, or impossible, to distinguish between different sources through a visual comparison of waveforms and/or PSDs. However, such distinction can become possible by grouping similar signals. Several statistical distances such as Euclidian, Mahalanobis, correlation, Kullback-Leibler distance, have been proposed as quantitative measures of "similarity" or "dissimilarity". To apply a chosen similarity measure, the parametric feature space should be defined. In the present work, the signals were grouped according to the likeness of their Fourier PSDs representing intrinsic properties of the signals. Various algorithms for AE signal categorization by joining the signals with similar PSDs and disjoining those with dissimilar PSD shapes have been proposed, c.f. [37-40]. Hierarchical *k*-means and fuzzy *c*-means procedures are admittedly the most popular [41]. The disadvantage of these algorithms is that the number of clusters to be derived must be set in advance. This number is usually not known *apriori*. Furthermore, it is difficult to handle outliers in data sets and the stability of *k*- or *c*-means may be seriously affected by outliers (spurious noise) which are omnipresent during tribological testing. This issue is address in the adaptive sequential *k*-means (ASK) scheme [39] and in the simplified method described below.

To compare the shapes of the AE spectral density functions and to make the results statistically independent of the signal power (or energy per frame) *W*, the area under the PSD curve was normalized to the total AE power measured in the frequency range from f_{min} to $f_{\max}$:

$$W = \int_{f_{\min}}^{f_{\max}} G(f)df \,, \tag{5}$$

i.e., the normalized power spectral density functions were obtained as

$$\tilde{G}(f) = G(f)/W \,. \tag{6}$$

Apparently, the integrals of $\tilde{G}(f)$ over the entire frequency range are equal to unity.

In the present work, a statistical quantity known as the *coefficient of determination R*^{2} was used as a measure K_S of pairwise similarity between $\tilde{G}(f)$ functions. The factor R^2 is computed in statistics [42] as:

$$\begin{aligned} R^2 &= \left(1 - \frac{\overline{S}_r^2}{\overline{S}_G^2}\right) \\ \overline{S}_r^2 &= \frac{\sum_{i=1}^{n} \left(g_{1i} - g_{2i}\right)^2}{n-2} \\ \overline{S}_G^2 &= \frac{\sum_{i=1}^{n} g_i^2 - \frac{1}{n}\left(\sum_{i=1}^{n} g_i\right)^2}{n-2} \end{aligned} \,, \tag{7}$$

where $\overline{S}_r^2$ is the residual variance; $\overline{S}_G^2$ is the total variance of the approximated PSD function *G*; g_{1i} and g_{2i} are discrete frequency components of the comparing PSD functions $G_1 = \left(g_{11} \dots g_{1i} \dots g_{1n}\right)$ and $G_2 = \left(g_{21} \dots g_{2i} \dots g_{2n}\right)$, respectively. This R^2 is a statistical similarity measure showing how close the data are to the fitted line. The smaller the variability of the residual values relative to the overall variability, the greater the similarity between the two comparing PSDs. For example, if there is no correlation between G_1 and G_2, then $\overline{S}_r^2 / \overline{S}_G^2 = 1, \quad R^2 = 0$, and vice versa, if G_1 and G_2 coincide, $\overline{S}_r^2 / \overline{S}_G^2 = 0, \quad R^2 = 1$.

Two PSDs G_1 and G_2 are said to be "similar" if the value R^2 computed according Eqs.(7) exceeds the preset "threshold" $\left[K_S\right]$, which plays the role of an acceptance criterion. They then are grouped to form a cluster of signals belonging to the same general population of sources. Obviously, there are no robust rules or mathematical guidelines for choosing the $\left[K_S\right]$ value. However, the choice of $\left[K_S\right]$ can be argued heuristically: the acceptance criterion $[K_S]$ should be set as conservative as possible (the larger the $[K_S]$ value, the more conservative the setting is) while the distinction between PSDs corresponding to different AE mechanisms is still possible. In this work, the cut-off $[K_S]$ value for the R^2 was set at 0.95. It is interesting to notice that a similar (in the statistical sense) approach was used by Williams and Egan in late 70th [43]. These authors employed a popular *t*-test to evaluate the difference between the means of two groups of AE spectra in attempt to classify the sources in fiber-reinforced composites.

The consistent relationship between critical points in the behavior of the tribo-system, AE signal groups, and the prevailing wear mechanisms was established through a comparison of the time of appearance of different group signals with direct observations of the worn surfaces in the interrupted tests. "Critical" points, *Pci*, are associated with time intervals, when one operating regime changes to another, i.e., when damage sets in after a period on normal "wear-less" operation, or when one prevailing wear mechanism transits to another, as illustrated in Fig. 3, for example. This figure represents the typical behavior of the integral AE parameter – waveform envelope – as a function of wear time which is superimposed with wear characteristics – friction coefficient and integral wear depth - measured concurrently by the tribometer during testing of the 100Cr6 steel. Critical points corresponding to familiar stages of wear – the beginning of adhesive wear and the beginning and ending of scuffing - are clearly identified by the transient behavior of the friction coefficient and the integral depth of wear. The integral AE parameter - envelope (or *rms* voltage) - reflects the same stages very reliably in excellent agreement with the early findings reported, e.g., in the above-cited refs. [8, 10-17].

At first, the wear test is conducted to failure and all "critical" (characteristic) points, *Pci*, which correspond to inflection points on the wear (or wear rate) curve and/or which are distinguishable by AE features, are identified as illustrated in Fig. 3. Then, a newly assembled tribosystem runs under the same conditions until AE parameters or their patterns become similar to those at the critical point in the first test. If several points of interest are identified, several tests are carried out using a new set of balls from the beginning to the point of interest. The test is interrupted at each critical point for microscopic surface observations. Timely test interruption by an AE signal enables microscopic examination of the fresh wear scar, identifying the underlying wear mechanism and its corresponding AE response [44]. The worn surface was analyzed using a confocal laser scanning microscope (CLSM) Olympus LEXT OLS4000 CLSM providing the 3-D imaging of finest details of the surface topology with the high resolution and good measuring capacity [45, 46].

4. Identifying AE Signatures of Critical Points and Wear Mechanisms

The proposed AE signal processing procedure permits efficient comparison of the protective properties of different lubricants for all the above-mentioned types of tribosystems and all testing modes. In what follows, the capacity of the proposed method will be illustrated by using the ASTM D2596 and D2783 standard tribological procedures [31, 32].

The AE clustering procedure shows that all AE signals fall naturally into three main categories differed statistically by the shapes of their normalized PSD functions. This was consistently observed regardless of the testing mode, tribosystem, and/or the grease used. Representative examples of the AE behavior in different friction and wear situations are shown in Figs. 4-7. Signals belonging to the first group are omnipresent and most numerous. The fraction of signals from this group was about 40-80% of the total number of detected AE signals. As will be shown below these signals are associated with friction noise. They can be filtered out and neglected in the analysis of the damage. Therefore, they are illustrated explicitly in Fig. 4, but are omitted in rest of figures for simplicity: as will be shown below, this group is related to friction noise and is not important for clarification of damage mechanisms. The second and third groups usually amount to about 10-40% and 4-20%, respectively. As will be shown below, in some rare situations, a single damage mechanism can dominate the AE appearance, so that, the fraction of signals of group 2 or 3 can approach 100%.

When the load on the tribosystem does not exceed the critical scuffing load, i.e. no scuffing occurs [4], only signals of groups 1 and 3 are recorded most commonly. Figs. 4a and 5. Under these conditions, the wear scar has a smooth mirror-like appearance with the presence of multiple small scratches and grooves in the sliding direction, Fig. 5a-d. The primary wear mechanism is associated with adhesive processes which signatures can be readily observed on microscopic CLSM images, Fig. 5. Some increase in the AE envelope values is systematically noticed under these conditions for different lubricants as wear progresses, c.f. Figs. 5e and f. However, the overall level of the AE signals is relatively low (compare to that shown in Fig. 6 for scuffing). Friction noise signals belonging to group 1 are filtered out in Figs. 5e and f. One can see that the signals from group 3 dominate during adhesive wear. Let us notice that under given conditions the scuffing was not observed since the size of the worn scar was smaller than the value tabulated in [31, 32] for scuffing at a given load.

The increase in load to the values close to the scuffing load is accompanied by a gradual increase in the total number of AE signals, Fig. 4b. The prevalence of the group 1 over the group 3 signals remains. The group 3 signals were observed predominantly at the beginning of the test. They are virtually not seen during initiation of scuffing, which is accompanied by a sharp increase of the AE envelope (cf. the scale on Figs. 4b-d, 5 and 6). During the post-scuffing running-in stage, the activity of the group 3 signals is low and tends to reduce to zero, Figs. 4a. The concomitant decrease in the AE envelope towards a steady value is systematically observed during this stage. As the testing load approaches the critical scuffing load, the AE envelope increases and fluctuates. Importantly is that at this time, the signals of group 2 appear often on a background of group 1 and 3 signals, which is indicative of imminent scuffing, Fig. 4b. Concurrently, deep scratches and grooves are formed within the worn scar as can be seen in interrupted tests, e.g. Fig. 6a. Larger adhesive spots, with overheated blue signatures, can be seen more frequently, Figs. 6b and c, as the load increases above the critical scuffing limit. Furthermore, when the signals of the group 2 appear, one can readily find severely plastically deformed areas at the edges of the worn scar, Fig. 6.

When the load on the sliding contact region was equal to or exceed the critical scuffing load, the pronounced AE envelope peak is observed, c.f. Figs. 3, 4b-d and 6e and f. At this stage, the AE level is several times greater than the initial AE level observed al lower loads or before scuffing occurs. The worn area is composed primarily of severely plastically deformed and plowed out metal in the direction of sliding, Fig. 6, and the dominant damage mechanism is associated with strongly localized plastic deformation. However, some microscopic cracks having the typical ductile morphology, Fig. 6c, and adhesive junctures with the overheated 'blue' appearance, Fig. 6b, can also be observed during the same stage. Besides, abrasive inclusions of the earlier spalled material are occasionally found buried in the contact surface at this stage, Fig. 7b. These findings appear in good agreement with the above-discussed thesis about the concurrent occurrence of multiple competing damage modes, which can be seen in different proportions at any time. Depending on testing conditions such as load, lubricants, contacting materials and surface finish, the contribution of individual mechanisms can be different. The proposed spectral categorization of AE signals can help to separate these contributions reasonably and reveal the prevailing damage mode.

Comparing the surface observation with the measured AE features, one can find that the developed scuffing is always accompanied by the group 2 signals, Fig. 4b-c, 6e-f, which are seen on a background of the signals from the group 1 (not shown in Fig. 6 for the reasons stated above). At the end of scuffing, the AE envelope, which has peaked during intensive scuffing, reduces to a lower constant level, Figs. 3, 4b, and 6e. Concurrently, the number of group 2 signals decreases progressively, until they vanish nearly entirely, which is indicative of completed running-in. When the test is stopped after this stage, the worn area has a smoothed appearance with a small number of grooves or with multiple shallow scratches similar to those shown in Fig. 6a. Most frequent and typical surface features are seen as layers of plastically deformed and plowed-out metal, Fig. 6d.

The main sources of each group of AE signals can be identified now. As has been noticed above, the group 1 signals is recognized in all tests and is most numerous. The activity of these signals is systematically seen from the onset of testing prior to scuffing and then it decreases and stabilizes at a constant level. The group 2 signals comes into play when severe wear or scuffing occurs. The peak activity or the maximum AE energy of the signals from this group always corresponds to scuffing, the severity of which is reflected by the height of the peak. This systematically observed feature of the AE behavior can serve as a reliable indicator of scuffing. Furthermore, since the signals of this group are regularly observed before scuffing occurs, their early identification can give some warning of impending scuffing and following galling. The activity of the group 2 AE signals gradually decreases to zero during the running-in stage. Scuffing usually develops quickly. However, when it continues over a relatively long period of time, a broad peak of AE envelope (or *rms* voltage) is observed as shown in Fig. 6e, f. The concomitant activity of the group 2 signals is steady but still high. The AE group 3 behaves very differently depending on load. The activity of this group usually increases on the early stage of testing, and then it gradually decreases until complete vanishing. Signals from this group are observed primarily before the occurrence of scuffing at the loads lower than the critical scuffing load; and their activity can increase slightly at this stage, as shown in Fig. 4b. This group of signals can also appear during the running-in stage.

By way of conclusion, based on the large volume of empirical data accumulated for different lubricants and tribosystems and on the above arguments correlating direct microscopic observations with AE signals, the AE sources can be broadly identified as follows:

- group 1 signals are produced by AE sources associated with friction noise caused by elastic-plastic asperity interactions and micro-scratching;

- group 2 signals are associated with the processes of intensive plastic deformation underlying scuffing in the tribological system [46];

- group 3 signals are associated with adhesive wear processes the formation and breaking of adhesive junctures.

5. Chronology of Wear Development (case study)

Lubricant selection is a long-standing problem which is typically solved on the basis of experience and knowledge. This approach becomes more and more challenging due to the increasing requirements for tribological components which are supposed to run faster, longer and experience higher loads. Reconstructing the chronology of damage occurrence, the AE is-situ condition monitoring adds considerable information to the selection procedure.

The proposed methodology of signal categorization and damage monitoring can be used to reconstruct the chronology of wear in a tribosystem from its inception to failure during testing of lubricants. Despite the different performance of lubricants, testing showed that damage occurred so that the worn surface relief was smoothed out quickly during running-in, following initial scuffing. Therefore, it is practically very difficult or even impossible to identify the prevailing degradation mechanism from post-mortem microscopic observations. On the other hand, the use of the suggested above AE-based workaround helps to determine a dominant wear damage mechanism and to restore the chronology of friction joint failure for different lubricants with a high degree of confidence.

Figure 7 illustrates the temporal AE-based characteristics of damage evolution represented by both the integral behavior of the AE envelope (or the *rms* voltage) and the spectral categorization of AE signals during the testing of different lubricants listed in Table 1 under step-wise loading in the standard four-ball machine. The chronology of the contact surface degradation was reconstructed by observing variation in the AE envelope with time, which was superimposed with the concurrent identification of characteristic groups of AE signals corresponding to individual damage mechanisms on different stages of damage development. The group 1 signals representing the friction noise is removed from Fig. 7 for the sake of clarity because they are not decisive for determination of the damage mechanism. One can clearly see that all lubricants behave considerably differently. Even the greases L5 (Fig. 7a) and L4 (Fig. 7b) having similar tribological properties (c.f. Table 1) respond differently to the same load. The AE signal revels that although both lubricants give rise to a similar size of the worn scars on the sliding surfaces, they behaved quite dissimilarly in time. Specifically, the AE signal categorization demonstrates that the AE time series is composed of transients belonging primarily to the group 3 (of course with the group 1 present too). This is indicative of the dominance of adhesive wear accompanied by plastic deformation of asperities and formation and breaking of adhesive junctions at the points of contact. However, the overall lubricating properties of L5 retained until the end of the test. With the grease L4, the picture is different in that multiple scuffing occurred obviously during testing. The first signature of scuffing was noticed as early as at the initial load of 392 N. Later, the second one appeared at the end of the test when load reached 981 N. Thus, friction degradation of the sliding surface started early and progressed throughout the test as could be seen by the gradually increasing size of the worn scar. Microscopic observations of the scars, which were performed during the interrupt testing, confirmed that the adhesive mechanism mediated the wear process involving the formation and rupture of adhesive junctions and local surface galling (c.f. also [44]). Thus, one can conclude that critical load when the lubricating film breaks down is quite low for the L4 grease (smaller than 392 N, which is appreciably smaller than that for the L5 grease – 588 N).

Similarly, Fig. 7 c-d illustrates the behavior of other lubricants listed in Table 1. Comparing the AE time-histories represented in terms of several parameters is a tedious task. For practical purposes, it is much more convenient to automate the analysis and symbolize the results by chronological bar chats shown in the lower parts of sub-figures in Fig. 7. In these charts, rows with colored (online) bars are assigned to different modes and damage mechanisms operating on different stages of the wear process. The rows A through E and the corresponding color (online) codes read as follows:

- Row A (dark blue online): indicates scuffing according to AE data. The relatively low AE envelope level is observed when the contacting surfaces are not severely damaged, e.g. at the beginning of the test. The AE envelope peak characterizes the time of initiation and termination of scuffing;
- Row B (red online): indicates the severity of damage according to microscopic observations; the row is empty as long as the wear scar size is smaller than the characteristic size of the scar formed during scuffing; the red bar corresponds to the time interval when significant damage sets in and size of the worn area is larger;
- Raw C (brown online): indicates the running-in stage. The characteristic AE envelope decay allows estimating the running-in time after scuffing;
- Rows D and E (light blue and yellow online, respectively): indicate the wear mechanisms. The AE cluster analysis dividing the whole set of signals into groups corresponding to different damage mechanisms allows evaluating the number of prevailing mechanisms of damage operative during the lifetime of the tribosystem, the time of their appearance and the sequence of their operation. Specifically, wear due to the formation and rupture of adhesive junctions is identified by the dominance of the AE group 3 signals in the time series (row D), wear by intensive plastic deformation is accompanied by the signals of group 2 (row E). Recall that scuffing is reliably identified when the activity and the energy of the signals from this group are high.

This procedure can be fully automated and used by practitioners in routine tribology testing for condition monitoring and express diagnostics of wear damage.

It should be noticed that the results of this work are strictly related to testing conditions so that the absolute values of measured parameters (amplitudes, energies, rms voltage, etc.) are case-sensitive. However, the ample experimental data presented confirm the strategic idea that if the proposed signal classification (or a like procedure) is adopted, regardless of inevitable numerical differences, there is a strong similarity in trends reported for signal separation into groups, their association with damage (wear) mechanisms and the timeline of wear progress in different tribosystems.

6. Summary and Conclusions

The combination of spectral and cluster analysis of AE time series continuously recorded during wear testing has proved efficient for deriving information about the lubricant performance and wear progression.

The increasing severity of wear is accompanied by a concomitant increase in the AE energy, which occurs in parallel with the decrease in the median frequency of the AE power-spectral density. The additional dimension provided by the AE spectral and cluster analysis offers a powerful means for the nondestructive assessment of wear mechanisms and identification of the prevailing one, even when several mechanisms coexist. The timing of occurrence of individual damage mechanisms can be reconstructed with high confidence and be used for predicting the imminent scuffing failure.

The proposed simple graphical presentation of the chronological timelines of contact surface degradation with the color-marked prevailing damage mechanisms can replace the complicated and cumbersome graphs combining multiple AE parameters without compromising their informative missions for practitioners. Since the applicability of the proposed approach is not limited to any particular tribosystem, this presentation substantially simplifies the routine friction and wear characterization and condition monitoring of industrial systems operating under variable conditions.

Acknowledgments
Financial support from the Ministry of Education and Science of Russian Federation through the contract № 11.8236.2017/9.10 is gratefully appreciated.

References

[1] H. S. Cheng, Section ed., “Lubricants and Lubrication,” ASM Handbook, Vol. 18: Friction, Lubrication, and Wear Technology, ed. P. J. Blau, ASM International, Materials Park, Ohio USA (1992) 79-171.
[2] V. Baranov, E. Kudryavtsev, G. Sarychev, V. Schavelin, Chapter 1 Friction of solids and nature of acoustic emission, in: B.J. Briscoe (Ed.) Tribology and Interface Engineering Series, Elsevier, Amsterdam, 2007, pp. 1-36.
[3] R.J. Boness, S.L. Mcbride, Adhesive and Abrasive Wear Studies Using Acoustic-Emission Techniques, Wear, 149 (1991) 41-53.
[4] R.J. Boness, S.L. Mcbride, M. Sobczyk, Wear Studies Using Acoustic-Emission Techniques, Tribol. Int., 23 (1990) 291-295.
[5] B. Bhushan, Y.J. Wu, N.S. Tambe, Sliding contact energy measurement using a calibrated acoustic emission transducer, IEEE Trans. Magn., 39 (2003) 881-887.
[6] J. Hanchi, B.E. Klamecki, Acoustic emission monitoring of the wear process, Wear, 145 (1991) 1-27.
[7] B.E. Klamecki, J. Hanchi, Wear Process Description Based on Acoustic-Emission, J. Tribol.-Trans. ASME, 112 (1990) 469-476.
[8] S. Lingard, C.W. Yu, C.F. Yau, Sliding Wear Studies Using Acoustic-Emission, Wear, 162 (1993) 597-604.
[9] N. Tandon, A. Choudhury, A review of vibration and acoustic measurement methods for the detection of defects in rolling element bearings, Tribol. Int., 32 (1999) 469-480.
[10] C.K. Mechefske, G. Sun, J. Sheasby, Using acoustic emission to monitor sliding wear, Insight, 44 (2002) 490-497.
[11] T. Hisakado, T. Warashina, Relationship between friction and wear properties and acoustic emission characteristics: iron pin on hardened bearing steel disk, Wear, 216 (1998) 1-7.
[12] S. Lingard, K.K. Ng, An Investigation of Acoustic-Emission in Sliding Friction and Wear of Metals, Wear, 130 (1989) 367-379.
[13] A. Morhain, D. Mba, Bearing defect diagnosis and acoustic emission, Proc. Inst. Mech. Eng. Part J J. Eng. Tribol., 217 (2003) 257-272.
[14] K. Matsuoka, D. Forrest, M.K. Tse, Online Wear Monitoring Using Acoustic-Emission, Wear, 162 (1993) 605-610.
[15] K. Matsuoka, K. Taniguchi, M. Nakakita, In-Situ wear monitoring of slider and disk using acoustic emission, J. Tribol., 123 (2001) 175-180.
[16] H.S. Benabdallah, D.A. Aguilar, Acoustic Emission and its Relationship with Friction and Wear for Sliding Contact, Tribol. Trans., 51 (2008) 738-747.
[17] H.S. Benabdallah, R.J. Boness, Tribological behaviour and acoustic emissions of alumina, silicon nitride and SAE52100 under dry sliding, Journal of Materials Science, 34 (1999) 4995-5004.
[18] J. Sun, R.J.K. Wood, L. Wang, I. Care, H.E.G. Powrie, Wear monitoring of bearing steel using electrostatic and acoustic emission techniques, Wear, 259 (2005) 1482-1489.
[19] Y.X. Yao, X.L. Li, Z.J. Yuan, Tool wear detection with fuzzy classification and wavelet fuzzy neural network, Int. J. Mach. Tool. Manufacturing, 39 (1999) 1525-1538.
[20] R.J. Kuo, P.H. Cohen, Intelligent tool wear estimation system through artificial neural networks and fuzzy modeling, Artificial Intelligence in Engineering, 12 (1998) 229-242.
[21] R.K. Dutta, S. Paul, A.B. Chattopadhyay, The efficacy of back propagation neural network with delta bar delta learning in predicting the wear of carbide inserts in face milling, Int. J. Adv. Manuf. Tec.h, 31 (2006) 434-442.

[22] E.D. Price, A.W. Lees, M.I. Friswell, Detection of severe sliding and pitting fatigue wear regimes through the use of broadband acoustic emission, Proc. Inst. Mech. Eng. Part J J. Eng. Tribol., 219 (2005) 85-98.
[23] A. Hase, H. Mishina, M. Wada, Correlation between features of acoustic emission signals and mechanical wear mechanisms, Wear, 292-293 (2012) 144-150.
[24] M.Y. Gokhale, D.K. Khanduja, Time Domain Signal Analysis Using Wavelet Packet Decomposition Approach, International Journal of Communications, Network and System Sciences, 3, 3 (2010) 9.
[25] J.L. Ferrando Chacon, V. Kappatos, W. Balachandran, T.-H. Gan, A novel approach for incipient defect detection in rolling bearings using acoustic emission technique, Applied Acoustics, 89 (2015) 88-100.
[26] F. Saeidi, S.A. Shevchik, K. Wasmer, Automatic detection of scuffing using acoustic emission, Tribol. Int., 94 (2016) 112-117.
[27] D. Baccar, D. Söffker, Wear detection by means of wavelet-based acoustic emission analysis, Mech. Syst. Signal Proc., 60-61 (2015) 198-207.
[28] S.A. Shevchik, F. Saeidi, B. Meylan, K. Wasmer, Prediction of failure in lubricated surfaces using acoustic time-frequency features and random forest algorithm, IEEE Trans. Ind. Inf., 13 (2017) 1541-1553.
[29] R.G. Bayer, Mechanical wear fundamentals and testing, Second ed., Marcel Dekker, New York, 2004.
[30] B. Bhushan, Modern tribology handbook, CRC Press, Boca Raton, FL, 2001.
[31] ASTM D2596-15, Standard Test Method for Measurement of Extreme-Pressure Properties of Lubricating Grease (Four-Ball Method), ASTM International, West Conshohocken, PA, 2015, www.astm.org.
[32] ASTM D2783-03(2014), Standard Test Method for Measurement of Extreme-Pressure Properties of Lubricating Fluids (Four-Ball Method), ASTM International, West Conshohocken, PA, 2014, www.astm.org, 2014.
[33] ASTM G99-17, Standard Test Method for Wear Testing with a Pin-on-Disk Apparatus, ASTM International, West Conshohocken, PA, 2017, www.astm.org.
[34] ASTM G77 - 17, Standard Test Method for Ranking Resistance of Materials to Sliding Wear Using Block-on-Ring Wear Test, Wear Test, ASTM International, West Conshohocken, PA, 2017, www.astm.org.
[35] J.S. Bendat, A.G. Piersol, Measurement and analysis of random data, Wiley, New York,, 1966.
[36] P.D. Welch, The Use of Fast Fourier Transform for the Estimation of Power Spectra: A Method Based on Time Averaging Over Short, Modified Periodograms, IEEE Transactions on Audio and Electroacoustics, 15 (1967) 70-73.
[37] D.L. Merson, A.A. Razuvaev, A.Y. Vinogradov, Application of the Spectral Analysis of Acoustic Emission Signals to Studies of Vulnerability of TiN Coatings on Steel Substrates, Russian Journal of Nondestructive Testing, 38 (2002) 508-516.
[38] I.A. Rastegaev, A.V. Danyuk, A.Y. Vinogradov, D.L. Merson, A.V. Chugunov, Location of noise-like sources of acoustic emissions using the spectral similarity method, Russian Journal of Nondestructive Testing, 49 (2013) 553-561.
[39] E. Pomponi, A. Vinogradov, A real-time approach to acoustic emission clustering, Mech. Syst. Signal Proc., 40 (2013) 791-804.
[40] A. Vinogradov, D.L. Merson, V. Patlan, S. Hashimoto, Effect of solid solution hardening and stacking fault energy on plastic flow and acoustic emission in Cu-Ge alloys, Materials Science and Engineering A, 341 (2003) 57-73.
[41] J.A. Hartigan, Clustering algorithms, Wiley, New York, 1975.
[42] J.L. Devore, Probability and statistics for engineering and the sciences, 8th ed, International Student ed., Brooks/Cole, Boston, Mass., 2012.
[43] J.H. Williams, D.M. Egan, Acoustic-Emission Spectral Analysis of Fiber Composite Failure Mechanisms, Materials Evaluation, 37 (1979) 43-47.

[44] I.A. Rastegaev, D.L. Merson, A. Vinogradov, Real time acoustic emission methodology in effective tribology testing, International Journal of Microstructure and Materials Properties, 9 (2014) 360-373.
[45] D.B. Hovis, A.H. Heuer, The use of laser scanning confocal microscopy (LSCM) in materials science, Journal of Microscopy, 240 (2010) 173-180.
[46] E. Merson, A.V. Kudrya, V.A. Trachenko, D. Merson, V. Danilov, A. Vinogradov, The Use of Confocal Laser Scanning Microscopy for the 3D Quantitative Characterization of Fracture Surfaces and Cleavage Facets, Procedia Structural Integrity, 2 (2016) 533-540.

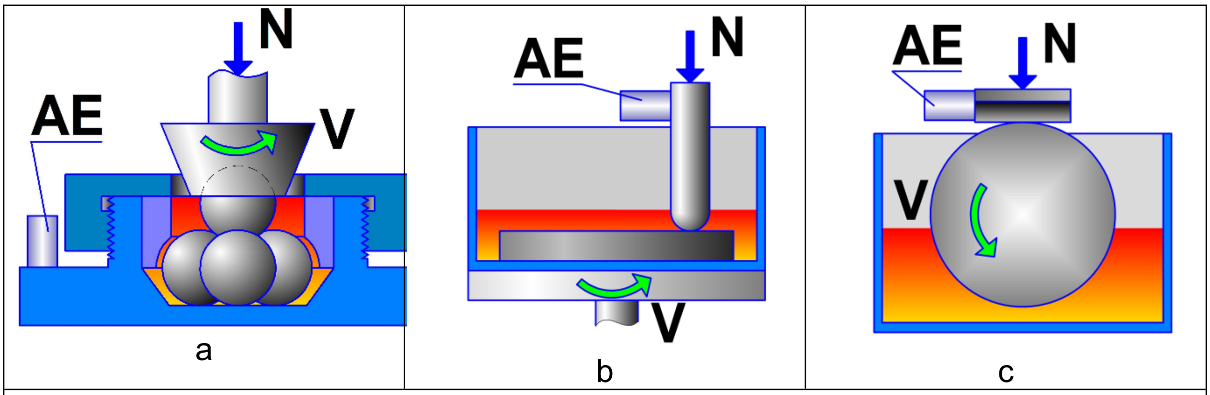

Figure 1. Schematic illustration of tribology testing methods: (a) four-ball [31, 32], (b) pin-on-disk [33], (c) cylinder-on-ring [34], N – stands for load and V for rotation direction.

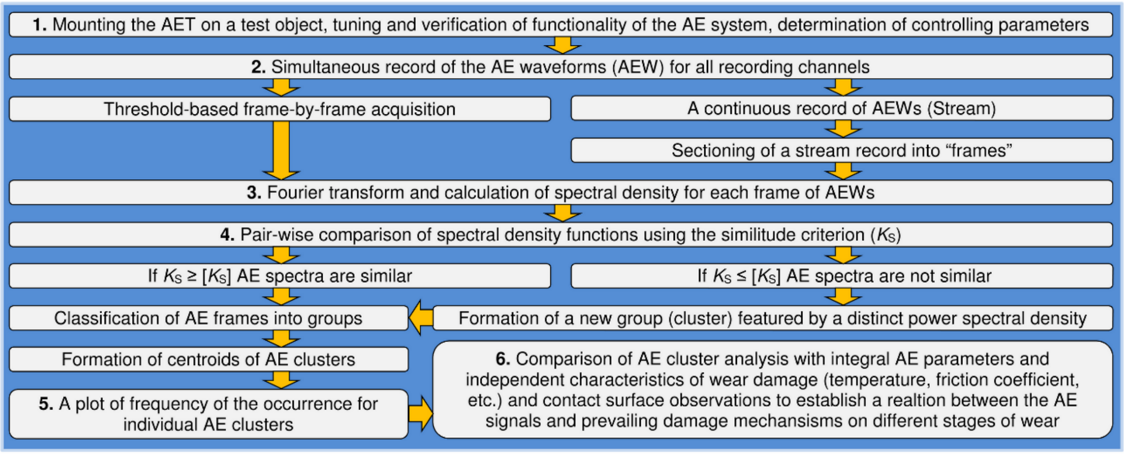

Figure 2. Workflow of non-supervised AE signal processing. AET stands for the AE transducer, AEW is the AE waveform, K_s is the calculated coefficient of similarity equal to the R^2 coefficient of approximation, $[K_s]$ is the threshold coefficient of similarity

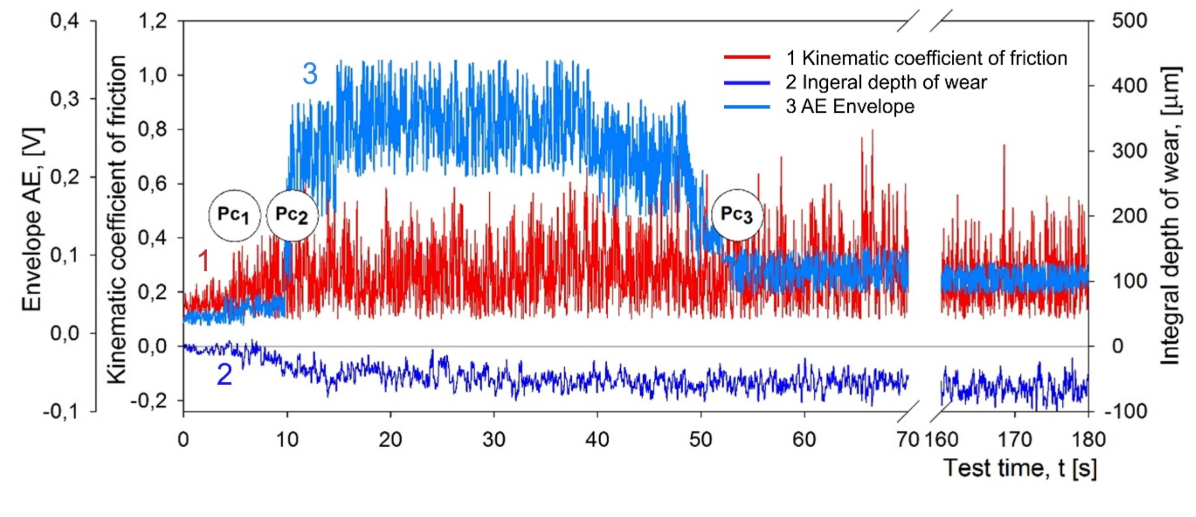

Figure 3. Typical behavior of the integral AE parameter – waveform envelope – as a function of wear time superimposed with wear characteristics – friction coefficient and integral wear depth - measured concurrently by the Nanovea TRB-50N tribometer during pin-on-disk testing of the steel C45 block according to the ASTM G99 standard of (ball indenter – steel 100Cr6, dry friction conditions, 10 N load, 150 rpm). Here *Pci* denotes critical points: Pc_1 corresponds to the onset of adhesive wear, Pc_2 indicates the onset of scuffing, Pc_3 indicates the end of scuffing and transition to a steady friction regime.

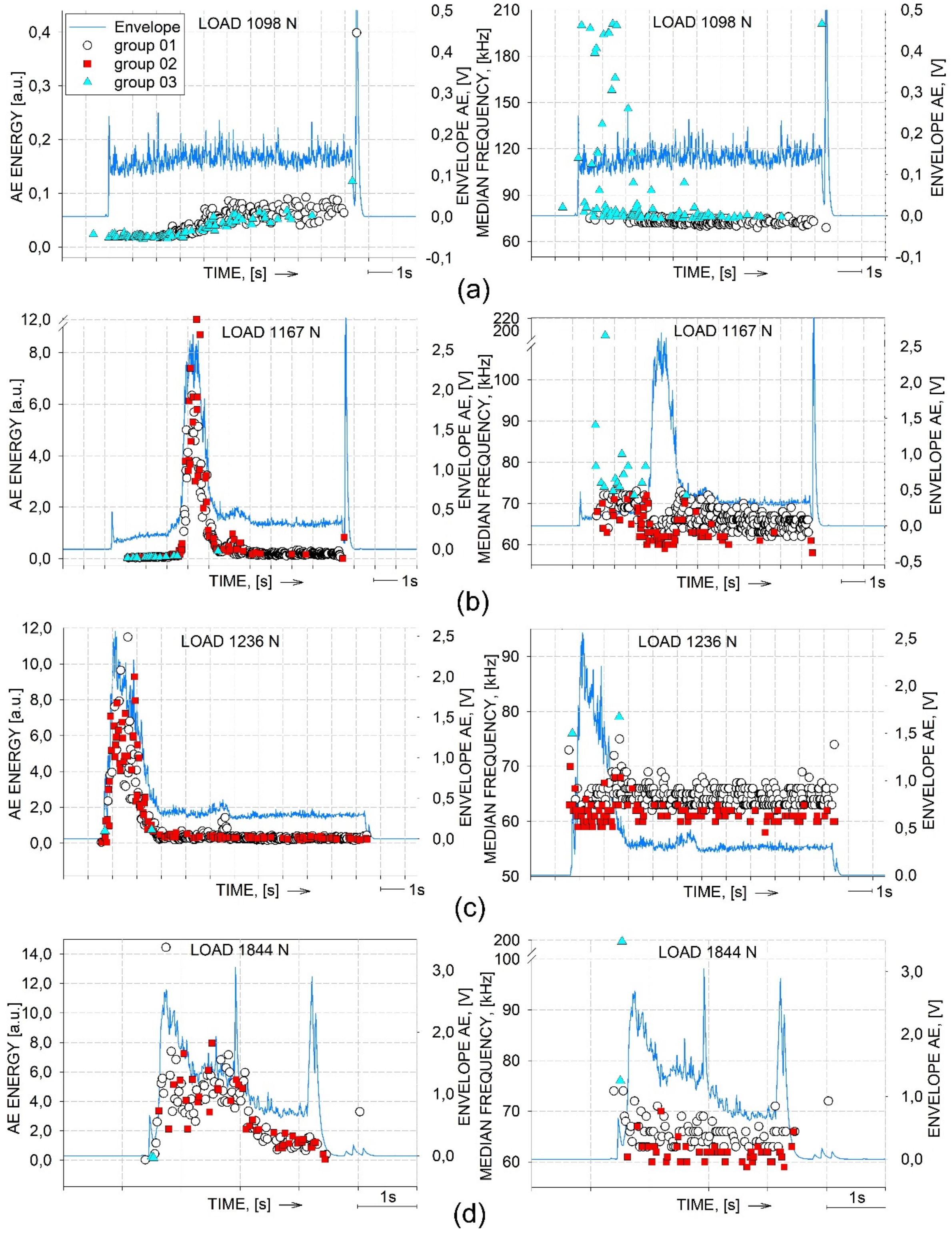

Figure 4. The AE energy and the PSD median frequency corresponding to different groups of AE signals as functions of time during four-ball wear test under different loads (motor oil designated as L6 in Table 1 is used a lubricant in these examples): (a) load is smaller than the critical scuffing load, (b) load is equal to the critical scuffing load, (c) load is above the critical scuffing load but is lower than the critical load for galling initiation, (d)

load is equal to the critical galling load. The legend shown in (a) applies to the entire figure.

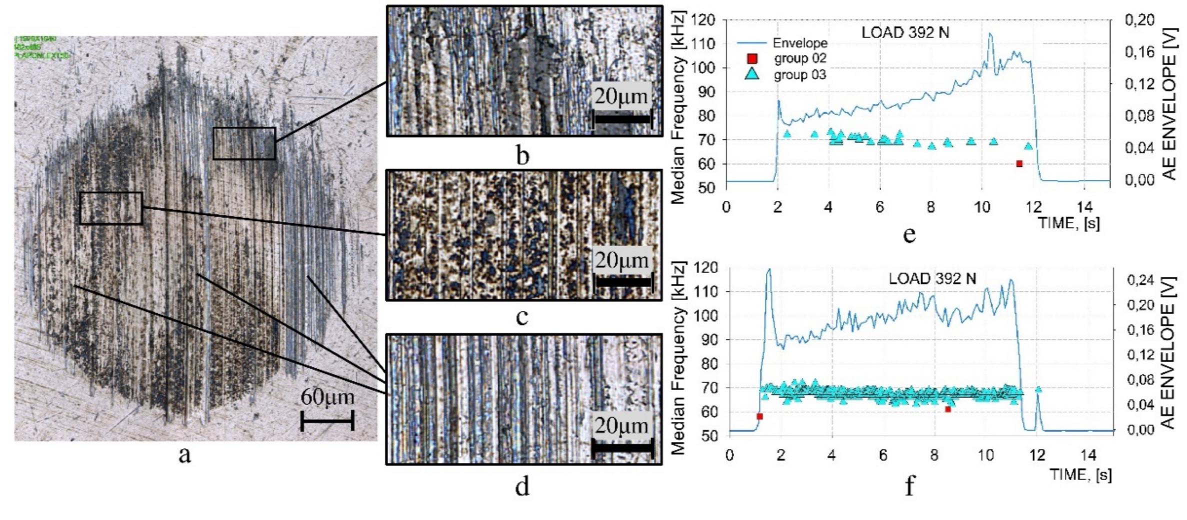

Figure 5. Typical CLSM microscopic image of the worn surface of the steel balls after four-ball tests (a) and magnified view of characteristic fragments corresponding to different damage mechanisms: (b) regions of adhesive wear, (c) adhesive points, (d) scratches. AE parameters – envelope and spectral median frequency during testing under loads slightly below the critical scuffing load for consistent greases with similar properties: (e) L3 and (f) L5, c.f. Table 1. The increase of the AE envelope values is systematically noticed under these conditions. The legend shown in (e) applies to both (e) and (f).

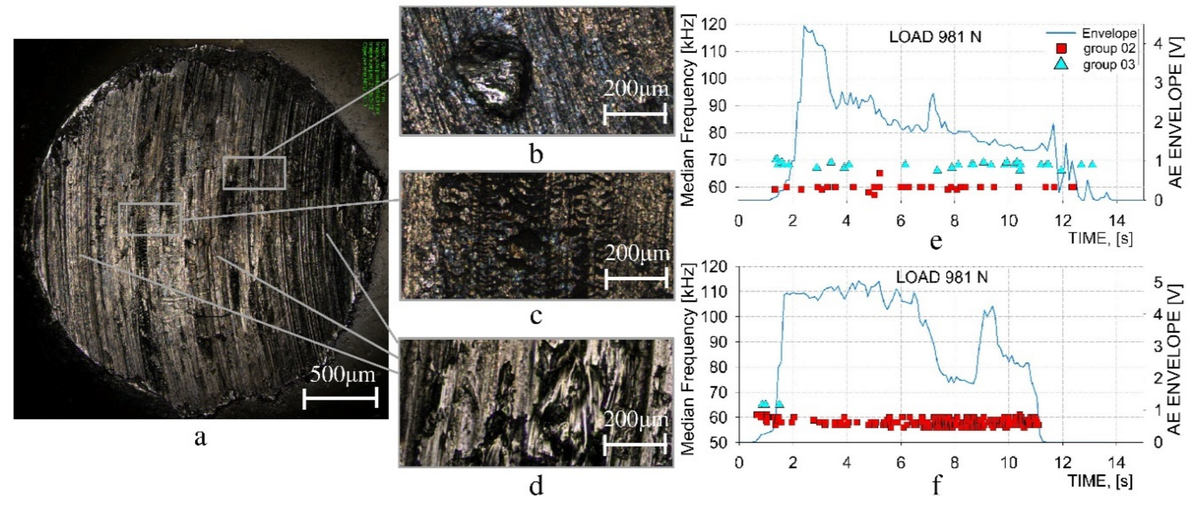

Figure 6. A typical microscopic image of the worn surface of 100Cr6 steel after four-ball testing (a) and magnified views of characteristic fragments corresponding to different damage mechanisms: (b) fragment of the heavily plastically deformed area with the overheat blue region and abrasive particle penetrated into the contact surface, (c) ductile cracks on the severely deformed surface, and (d) layers of plastically deformed material. Corresponding AE parameters during testing under loads above the critical scuffing load for consistent greases with similar properties: (e) L3 and (f) L5 (c.f. Table 1). The legend shown in (e) applies to both (e) and (f).

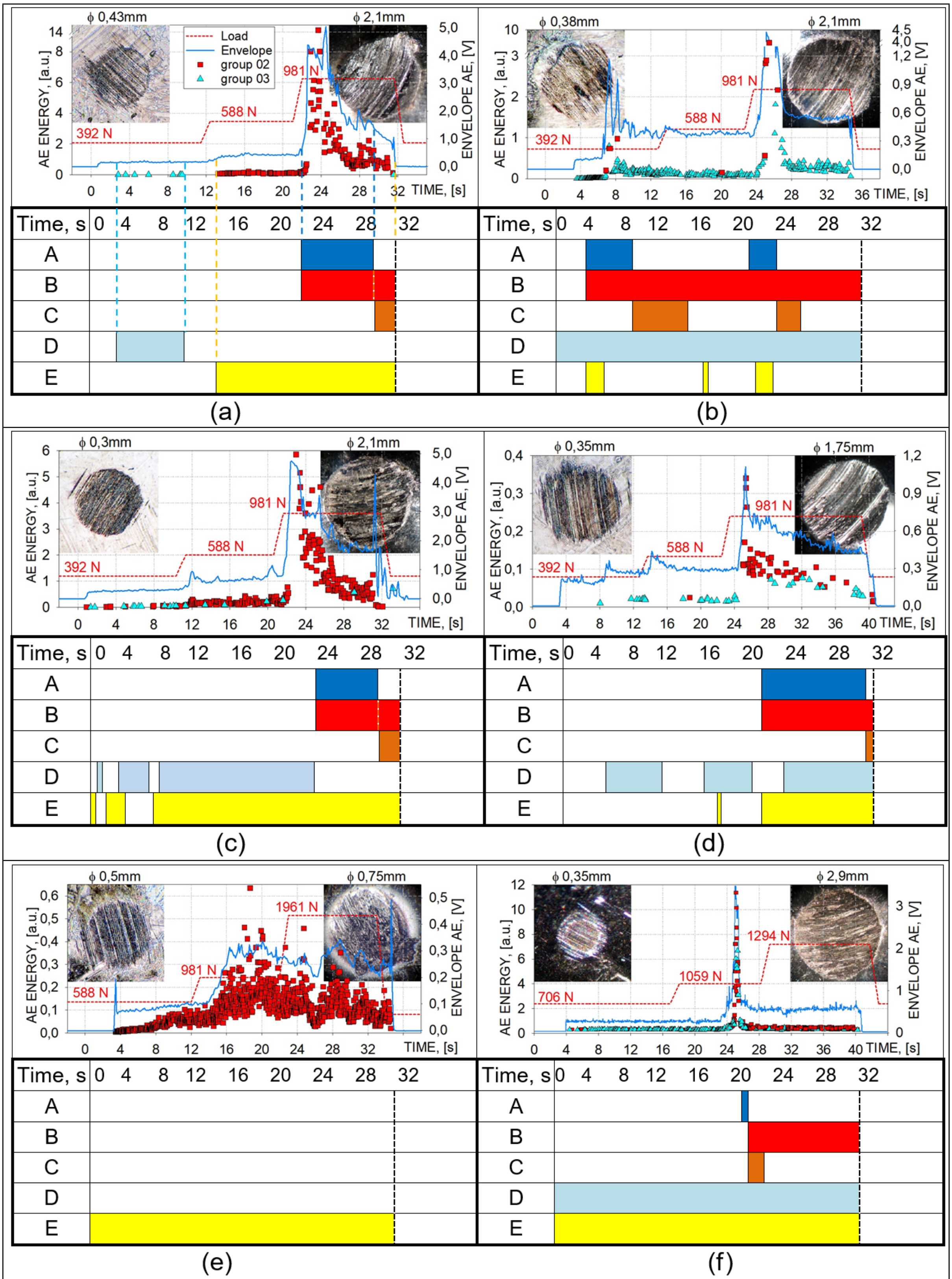

Figure 7. Typical graphs showing the AE behavior and corresponding chronological damage in four-ball testing of 100Cr6 steel with different greases: (a) L5, (b) L4, (c) L3, (d) L2, (e) L1, (f) L6, listed in Table 1. The legend shown in (a) applies to the entire figure. CLSM micrographs on the left hand side and on the right hand side of each sub-figure illustrate

the scar morphology and its diameter before and after scuffing. The colored (online) bar chats illustrate different stages of wear damage (onset and termination) and corresponding wear mechanisms in the tribosystem revealed by the non-supervised automated AE analysis (see text for details):

A - the scuffing stage according to AE data

B - the damage status bar: the red (online) bar in this raw denotes severe damage (scuffing) according to microscopic observation of the worn area

C - the running-in stage

D - wear dominated by the adhesive mechanism

E - wear dominated by intensive plastic deformation

Table 1. Properties of lubricants tested

Designation	Tradename	Types of lubricants	Base oil	Thickener	Solid additive	Viscosity base oil, cSt (+40°C)	Penetration, 0.1mm (+25°C)	Tribological characteristics [30][31] (+25°C)		
								Load-Wear Index, N	Last nonseizure load, N	Weld Load, N
L1	SHRUS-4M	grease	mineral	Lithium 12-hydroxystearate	MoS_2	150	270	770	1200	6300
L2	Renolit IP 1619	grease	synthetic		-	25	320	360	840	2370
L3	Litol-24	grease	mineral		-	65	230	280	630	1600
L4	Unirex-3	grease	mineral		-	115	235	300	710	2240
L5	Fiol-1	grease	mineral		-	50	320	310	800	1780
L6	Lukoil (motor oil)	liquid	mineral	-	-	90	-	970	1190	1880

Author’s Agreement

On behalf of all co-authors, I am to certify that the content of this paper is our own work. All authors are aware of the content and agree to publish it in Wear. This manuscript has not been submitted to any other journal or conference proceedings. I certify that the all the assistance received in preparing this manuscript and sources of funding have been acknowledged.

Alexei Vinogradov